Mon. Not. R. Astron. Soc. **000**, 1–8 (0000) Printed 6 June 2016 (MN LATEX style file v2.2)

On the properties of compact groups identified in different photometric bands

Antonela Taverna[1⋆], Eugenia Díaz-Giménez[1,2], Ariel Zandivarez[1,2], Francisco Joray[3], María José Kanagusuku[1]

1 *Instituto de Astronomía Teórica y Experimental (IATE), UNC, CONICET, OAC, Córdoba, Argentina.*
2 *Observatorio Astronómico (OAC), Universidad Nacional de Córdoba (UNC), Laprida 854, X5000BGR, Córdoba, Argentina.*
3 *Facultad de Matemática, Astronomía y Física (FaMAF), UNC.*

arXiv:1606.01184v1 [astro-ph.GA] 3 Jun 2016

6 June 2016

ABSTRACT

Historically, compact group catalogues vary not only in their identification algorithms and selection functions, but also in their photometric bands. Differences between compact group catalogues have been reported. However, it is difficult to assess the impact of the photometric band in these differences given the variety of identification algorithms. We used the mock lightcone built by Henriques et al. (2012) to identify and compare compact groups in three different photometric bands: K, r, and u. We applied the same selection functions in the three bands, and found that compact groups in the u-band look the smallest in projection, the difference between the two brightest galaxies is the largest in the K-band, while compact groups in the r-band present the lowest compactness. We also investigated the differences between samples when galaxies are selected only in one particular band (*pure* compact groups) and those that exist regardless the band in which galaxies were observed (*common* compact groups). We found that the differences between the total samples are magnified, but also some others arise: pure-r compact groups are the largest in projection; pure-u compact groups have the brightest first ranked galaxies, and the most similar two first ranked galaxies; pure-K compact groups have the highest compactness and the most different two first ranked galaxies; and common compact groups show the largest percentage of physically dense groups. Therefore, without a careful selection and identification of the samples, the characteristic features of group properties in a particular photometric band could be overshadowed.

Key words: galaxies: clusters: general – methods: statistical – methods: data analysis

1 INTRODUCTION

Given their extreme nature, compact groups (CGs) are one the favourite objects in extragalactic astronomy to study galaxy formation and evolution. Galaxy interactions are supposed to occur more likely within these small system of galaxies, hence important clues about galaxy evolution can be obtained from the analysis of the physical properties of the galaxy members and their host groups.

During the last fifty years, several attempts have been done to construct CGs catalogues, providing the possibility of performing comparisons of the CG physical properties among different catalogues. Starting with the pioneer attempt of Rose (1977) and the well known catalogue of Hickson (1982), several other authors have embarked themselves in the work of building CGs catalogues, such as Prandoni et al. (1994); McConnachie et al. (2009); Díaz-Giménez et al. (2012) and Hernández-Fernández & Mendes de Oliveira (2015). We mention only these particular catalogues because they are examples of surveys characterised by galaxy detections with different photometry: B (Johnson & Morgan 1953), R (Cousins 1976), b_j (COSMOS-UKST, Yentis et al. 1992), r (Sloan Digital Sky Survey, SDSS, York & SDSS Collaboration 2000), K_s (Two Micron All-Sky Survey, 2MASS, Skrutskie et al. 2006) and FUV (Galaxy Evolution Explorer, GALEX, Bianchi 2014) bands. All these surveys span a wide range of the electromagnetic spectrum (roughly from 1400 to 23000 Å), implying that objects with very different physical properties could be detected depending on which part of the spectrum is adopted to construct the galaxy surveys. Also, the different selection functions of the surveys (e.g., apparent magnitude limits, sky coverage) and algorithms to identify CGs (e.g., visual or automatic search, Hickson-like or friends-of-friends - FoF - type, with or without velocity filter) are very uneven among the existing CG catalogues. Hence, all these issues con-

⋆ antotaverna@gmail.com

© 0000 RAS

tribute to make the comparison among different samples of CGs a difficult task.

For instance, Díaz-Giménez et al. (2012) compared the samples of CGs identified by themselves in the K-band (automatic Hickson-like plus flux limit algorithm) with the samples of CGs identified in the B band (Focardi & Kelm 2002, FoF-like algorithm), and in the R-band (Allam & Tucker 2000, FoF algorithm; and Hickson et al. 1992, visual inspection). They found that CGs in the R-band have smaller projected sizes, projected intergalaxy separations and crossing times than the other two catalogues. They also found that the K-sample was the first to show statistically large first–second ranked galaxy magnitude gap. Hernández-Fernández & Mendes de Oliveira (2015) have also performed a comparative analysis between the CGs identified by themselves from ultraviolet sources (SFCG, FoF algorithm on the plane of sky) with the samples of CGs in the K-band (Díaz-Giménez et al. 2012), R-band (Hickson et al. 1992) and in the r-band (McConnachie et al. 2009, automatic Hickson-like algorithm). They found that the SFCGs present the lowest velocity dispersions (and virial masses), while the R-CGs present the smallest projected intergalaxy separations and crossing times. Nevertheless, given the differences in the identification processes, it is hard to tell which is the nature of those differences. Therefore, a fair comparison among different samples of CGs is required.

Semi-analytic models of galaxy formation combined with N-body numerical simulations have proved to be efficient at reproducing the properties of CGs in different bands (e.g., McConnachie et al. 2009; Díaz-Giménez & Mamon 2010). Therefore, in this work we use an all-sky lightcone (Henriques et al. 2012) constructed using the semi-analytic galaxies extracted from the Millennium Simulation (Springel et al. 2005) to identify CGs in three different photometric bands: u (SDSS) , r (SDSS) and K_s (2MASS). This will allow us to standardise the conditions for the identification of CGs and performing a comparison among the resulting samples of CGs. This should shed some light on whether those differences observed in previous observational identifications are caused by using different algorithms and restrictions to identify CGs, an unfair or biased comparison among samples, or if CGs in different photometric bands are intrinsically different.

The layout of this work is as follows: we describe the mock catalogue, the compact group identifications and the analysis of their properties in Section 2. In Sect. 3, we split the sample of CGs into those that exist regardless the photometric band, and those that only exist in one particular band, and we compare their properties. Finally, in Section 4 we summarise our results and conclusions.

2 THE COMPACT GROUP SAMPLES

2.1 The mock catalogue

We identified compact groups of galaxies in the publicly available all-sky lightcone built by Henriques et al. (2012)[1]. Those authors constructed the lightcone using the semi-analytic galaxies extracted from the Guo et al. (2011) by replicating the Millennium simulation box ($500\ \mathrm{Mpc\ h^{-1}}$ on a side), and selecting galaxies from the different outputs of the simulation to include the evolution of structures and galaxy properties with time. The semi-analytic model of galaxy formation of Guo et al. (2011) introduced several modifications with respect to earlier models. For instance, they introduced changes in the treatments of gas accretion, SN feedback, sizes of galaxies, and stripping of gas and stars. The implementation of these modifications led them to a model that reproduces very well the observed abundance and the large-scale clustering of low redshift galaxies as a function of stellar mass, luminosity and colour, and also reproduces the colour distribution and the small-scale clustering of SDSS galaxies.

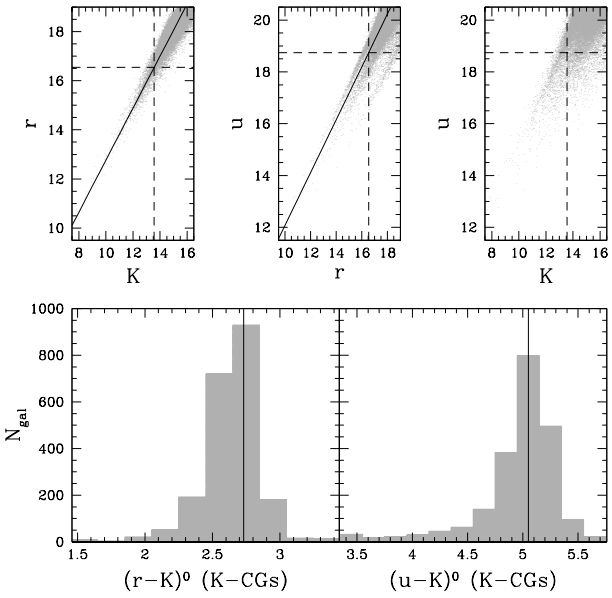

Figure 1. Top panels: galaxy magnitudes in the parent lightcone (only 0.05% of the original points are plotted). Solid lines represent the linear fit to the data, while dashed lines represent the limit adopted in each band. Bottom panels: distribution of differences between the rest frame apparent magnitudes in two different photometric bands of galaxies in Compact Groups identified in the K-band (Sect. 2.2). Solid lines represent the values adopted to determine the band shift to compute the surface brightness limit.

Henriques et al. (2012)'s original mock lightcone is limited to an apparent observer-frame AB magnitude of $i < 21.0$ and includes apparent observer-frame magnitudes for 9 filters: SDSS u, g, r, i, z and VISTA Y, J, H, Ks. In this work, we focused in three of these bands: Ks[2], r, and u.

To mimic the observational sample of compact groups identified in a previous work in the 2MASS catalogue (Díaz-Giménez et al. 2012), we converted the apparent K(AB) band available for the mock galaxies from the AB system to the Vega system to match the 2MASS magnitudes: $K(\mathrm{Vega}) = K(\mathrm{AB}) - 1.85$ (Cohen et al. 2003; Targett et al. 2012), and selected galaxies down to an apparent magnitude limit of $K = 13.57$. The sample comprises 701449 galaxies within a solid angle of $4\,\pi$. The number density of this particular mock galaxy catalogue reproduces the number density observed in the 2MASS catalogue remarkably well. We also selected mock galaxy catalogues in the u- and in the r-bands. The apparent magnitude limits imposed in each of these bands were determined in order to mimic the limit in the K-band. Therefore, we examined the distribution of magnitudes in the three bands. Top panels in Fig. 1 show the scatter plots of galaxy magnitudes: K vs.

[1] Galaxy mock lightcone available as table wmap1.BC03_AllSky_001 at http://www.mpa-garching.mpg.de/millennium/

[2] Hereafter, we will refer to this magnitude just as K instead of Ks

Table 1. Main parameters used to select galaxies in the mock catalogues, identify compact groups in different photometric bands, and assign sizes to the simulation particles.

	K	r	u
$m_{\rm lim}$	13.57	16.54	18.73
# galaxies	701449	677351	928367
$< z >$	0.065	0.057	0.063
$m_{\rm bri_{lim}}$	10.57	13.54	15.73
Band shift	...	r=K+2.73	u=K+5.05
$\mu_{\rm lim}$	23.6	26.33	28.65
$M_{\odot}^{(1)}$	3.29	4.65	6.44
$\alpha^{(2)}$	0.11	0.11	0.12
$\beta^{(2)}$	0.72	0.78	0.69
$\gamma^{(2)}$	0.09	0.12	0.11
$\mathcal{M}_0^{(2)}$	1.57×10^{10}	2.25×10^{10}	1.70×10^{10}
$a^{(2)}$	20.45×10^{-3}	37.24×10^{-3}	23.75×10^{-3}
$b^{(2)}$	0.22	0.20	0.23

Notes. (1) www.ucolick.org/∼cnaw/sun.html; (2) Prescriptions from Lange et al. (2015) to compute the galaxy half-light radii (R_i) as a function of the stellar mass ($\mathcal{M}_i^*$). Elliptical galaxies: $R_i = \gamma\,(\mathcal{M}_i^*)^{\alpha}(1 + \mathcal{M}_i^*/\mathcal{M}_0)^{(\beta-\alpha)}$. Non-elliptical galaxies: $R_i = a(\mathcal{M}_i^*)^b$

Table 2. Group properties for the total and restricted samples of CGs

	Total Samples			Restricted Samples		
Sample	K	r	u	K	$\tilde{\rm r}$	$\tilde{\rm u}$
# CG	447	406	276	382	289	231
θ_G	3.2 (0.2)	3.4 (0.2)	3.5 (0.3)	3.3 (0.2)	3.7 (0.2)	3.5 (0.3)
r_p	67 (3)	72 (3)	66 (4)	65 (3)	73 (4)	62 (4)
$R_{\rm vir}$	90 (5)	106 (5)	96 (7)	86 (5)	102 (6)	93 (7)
$\langle d_{ij} \rangle$	73 (4)	82 (4)	73 (5)	72 (4)	81 (4)	70 (4)
$s_\perp$	105 (6)	117 (6)	113 (8)	102 (6)	114 (8)	101 (7)
$s_\parallel$	103 (14)	119 (17)	156 (31)	99 (14)	117 (19)	140 (28)
s_4	168 (15)	182 (16)	205 (27)	162 (15)	180 (19)	187 (24)
σ_v	280 (14)	281 (15)	253 (21)	270 (15)	284 (18)	265 (22)
$H_0\,t_{\rm cr}$	2.7 (0.2)	2.9 (0.3)	2.9 (0.4)	2.7 (0.2)	2.8 (0.3)	2.6 (0.3)
$\mathcal{M}_{\rm vir}$	6.9 (0.9)	7.3 (1.1)	6.5 (1.4)	6.3 (0.9)	7.8 (1.4)	6.5 (1.4)
$K_{\rm bri}$	10.0 (0.1)	10.2 (0.1)	9.9 (0.1)	9.9 (0.1)	9.9 (0.1)	9.8 (0.1)
$r_{\rm bri}$	12.8 (0.1)	13.0 (0.1)	12.6 (0.1)	12.7 (0.1)	12.7 (0.1)	12.6 (0.1)
$u_{\rm bri}$	15.2 (0.1)	15.3 (0.1)	15.0 (0.1)	15.1 (0.1)	15.0 (0.1)	14.9 (0.1)
ΔK_{12}	1.3 (0.1)	1.2 (0.1)	1.1 (0.1)	1.3 (0.1)	1.2 (0.1)	1.1 (0.1)
Δr_{12}	1.3 (0.1)	1.2 (0.1)	1.0 (0.1)	1.3 (0.1)	1.2 (0.1)	1.1 (0.1)
Δu_{12}	1.3 (0.1)	1.2 (0.1)	1.1 (0.1)	1.3 (0.1)	1.2 (0.1)	1.1 (0.1)
μ_K	21.9 (0.1)	22.2 (0.1)	22.1 (0.1)	21.9 (0.1)	22.2 (0.1)	21.8 (0.1)
μ_r	24.8 (0.1)	25.1 (0.1)	24.9 (0.1)	24.7 (0.1)	25.1 (0.1)	24.7 (0.1)
μ_u	27.1 (0.1)	27.4 (0.1)	27.2 (0.1)	27.1 (0.1)	27.4 (0.1)	27.0 (0.1)
L_K	231 (14)	219 (15)	194 (18)	227 (14)	224 (19)	207 (18)
L_r	68 (4)	66 (4)	59 (4)	67 (4)	67 (5)	61 (5)
L_u	41 (3)	41 (3)	44 (4)	41 (3)	42 (4)	41 (3)
$\mathcal{M}_{\rm v}/L_K$	29 (3)	32 (4)	32 (6)	27 (3)	30 (5)	30 (5)
$\mathcal{M}_{\rm v}/L_r$	100 (11)	109 (14)	106 (19)	94 (12)	104 (17)	103 (19)
$\mathcal{M}_{\rm v}/L_u$	158 (20)	178 (24)	161 (27)	136 (20)	174 (30)	167 (30)
$T1_K$	0.56 (0.03)	0.56 (0.03)	0.75 (0.04)	0.54 (0.02)	0.54 (0.03)	0.65 (0.04)
$T2_K$	0.61 (0.02)	0.61 (0.02)	0.68 (0.03)	0.61 (0.02)	0.61 (0.03)	0.65 (0.03)
$T1_r$	0.56 (0.02)	0.57 (0.02)	0.72 (0.04)	0.54 (0.02)	0.56 (0.03)	0.64 (0.03)
$T2_r$	0.61 (0.02)	0.61 (0.02)	0.67 (0.03)	0.59 (0.02)	0.60 (0.03)	0.63 (0.03)
$T1_u$	0.63 (0.03)	0.66 (0.03)	0.71 (0.04)	0.61 (0.03)	0.65 (0.03)	0.68 (0.04)
$T2_u$	0.67 (0.02)	0.71 (0.03)	0.69 (0.03)	0.66 (0.03)	0.70 (0.03)	0.66 (0.03)
% Reals	55.6	52.0	44.4	57.9	52.2	48.9

Notes: In each cell, the format xx (ss) contains the median (xx) and the shift (ss) to construct an approximated 95% confidence interval, $CI = xx \pm ss$ (see text for details), except for the T_1 and T_2 values where the quantity in parentheses are the error bars computed using the bootstrap resampling technique. Units: θ_G = arcmin; r_p, $R_{\rm vir}$, $\langle d_{\rm ij} \rangle$, $s_\perp$, $s_\parallel$ and s_4 = kpc h^{-1}; σ_v = km s^{-1} ; $H_0\,t_{\rm cr} = 10^{-2}$; $\mathcal{M}_{\rm vir} = 10^{12}\ \mathcal{M}_\odot$ h^{-1} ; magnitude gaps are calculated in absolute magnitudes for each photometric band; μ = mag/arcsec^2; $L = 10^9\ L_\odot$ h^{-2}; $\mathcal{M}_{\rm vir}/L = {\rm h}\,\mathcal{M}_\odot/L_\odot$.

r (left panel), u vs. r (middle panel), and K vs u (right panel). Using a linear fit for K vs. r, we determined the r-band magnitude limit corresponding to $K_{\rm lim} = 13.57$, which led us to $r_{\rm lim} = 16.54$. To determine the limit in the u-band, we fit the distribution u vs. r[3]. For $r_{\rm lim} = 16.54$, we found $u_{\rm lim} = 18.73$. Given the spread of the distributions around the linear fits, adopting a fixed magnitude limit in one or another band inevitably leads to a different galaxy sampling towards the fainter magnitudes. This is a fact that is also present in the observational catalogues limited by flux, as many of the catalogues used in the literature to identify CGs in different bands. We will also explore how this affect the samples of CGs extracted from each catalogue. The number of galaxies comprised in each mock catalogue are quoted in Table 1.

2.2 The compact group identification

We identified mock CGs in the galaxy lightcones using the criteria defined by Díaz-Giménez et al. (2012):

- Population: $4 \leqslant N \leqslant 10$
- Compactness: $\mu \leqslant \mu_{\rm lim}$ [mag/arcsec^{-2}]
- Isolation: $\Theta_N > 3\Theta_G$
- Flux limit: $m_{\rm bri} \leqslant m_{\rm lim} - 3$
- Velocity filtering: $|v_i - < v >| \leqslant 1000\,{\rm km\,s^{-1}}$

where N is the number of galaxies whose K-band magnitudes are within a 3-magnitude range from the brightest galaxy, $m_{\rm bri}$ is the apparent magnitude of the brightest galaxy of the group; μ is the mean surface brightness in a given band, averaged over the smallest circle that circumscribes the galaxy centres; Θ_G is the angular diameter of the smallest circumscribed circle; Θ_N is the angular diameter of the largest concentric circle that contains no other galaxies within the considered magnitude range or brighter; v_i is the radial velocity of each galaxy member and $< v >$ is the median of the radial velocity of the members. In Table 1 we show the limits adopted in each band for the compactness and flux limit criteria. In the K-band, we adopted the values described in Díaz-Giménez et al. (2012). To determine the limiting value for the compactness criterion in the other two bands, following Díaz-Giménez et al. (2012), we examined the resulting sample of CGs identified in the K-band and determined the mean band shifts: $(r-K)^0 = 2.73$ and $(u-K)^0 = 5.05$. These are shown with solid lines in the bottom panels of Fig 1. Using these values we shifted the corresponding μ value in the K band to obtain the corresponding values in the other two bands. We also checked for CGs embedded within larger CGs that also meet the criteria described above. Following Díaz-Giménez & Mamon (2010), for such groups, we kept the larger group (for a complete description of the algorithm, see Figure 1 in that paper).

We have also considered the fact that galaxies in the mock catalogues are just point-sized particles, therefore we have included the blending of galaxies in projection on the plane of the sky which modify the number of detectable objects, changing the population of the compact groups. According to the morphological type of each galaxy - determined based on the ratio of stellar mass of the bulge and the total stellar mass (Bertone et al. 2007) -, we computed their half-light radii in each band as a function of the stellar mass of each mock galaxy following the prescriptions of Lange et al. (2015) (see Table 1). Finally, we considered two galaxies as blended if the angular separation between the two galaxies is smaller than the sum of their angular half-light radii.

[3] Instead of using the 'u vs. K' distribution, we chose using 'u vs. r' to make the linear fit since it has smaller dispersion

Within a solid angle of 4π, we identified 447 CGs in the K-band (K-CGs), 406 in the r-band (r-CGs), and 276 in the u-band (u-CGs).

2.3 Compact group properties

We measured several group properties that will be used to compare the three CG samples. These properties are:

- θ_G: angular diameter of the minimum circle that encloses all the group members
- r_p: projected radius of the minimum circle
- $R_{\rm vir}$: projected virial radius of the group computed as $R_{\rm vir} = 2N(N-1)(\sum_{ij}\frac{1}{d_{ij}})^{-1}$ where d_{ij} are the projected separations between galaxies.
- $\langle d_{ij}\rangle$: median of the projected intergalaxy separations
- $s_\perp$: maximum projected separation between the four closest galaxies
- $s_\parallel$: maximum comoving line-of-sight separation between the four closest galaxies.
- s_4: 3D comoving maximum interparticle separation between the four closest galaxies
- σ_v: group gapper radial velocity dispersion
- $H_0\,t_{\rm cr}$: dimensionless crossing time computed as $H_0\,t_{\rm cr} = \frac{\pi{\rm x}100\ {\rm h}}{2\sqrt{3}}\frac{\langle d_{ij}\rangle}{\sigma_v}$
- $\mathcal{M}_{\rm vir}$: virial mass computed as $\mathcal{M}_{\rm vir} = \frac{3\pi}{2G}R_{\rm vir}\,\sigma_v^2$
- $K_{\rm bri}$, $r_{\rm bri}$, $u_{\rm bri}$: observer frame apparent magnitude of the brightest galaxy in the three bands
- ΔK_{12}, Δr_{12}, Δu_{12}: rest frame absolute magnitude difference between the first- and the second-ranked galaxies
- μ_K, μ_r, μ_u: group surface brightness in the three bands
- L_K, L_r, L_u: total group luminosity in the three bands
- $\mathcal{M}_{\rm v}/L_K$, $\mathcal{M}_{\rm v}/L_r$, $\mathcal{M}_{\rm v}/L_u$: mass-to-light ratio in the three bands

We also computed for each sample and in each band, the Tremaine-Richstone statistics, T1 and T2 (Tremaine & Richstone 1977):

$$T1 = \frac{\sigma(M_1)}{< M_2 - M_1 >}, \quad T2 = \frac{1}{\sqrt{0.677}}\frac{\sigma(M_2 - M_1)}{< M_2 - M_1 >}$$

Groups with a first-ranked galaxy much brighter than the second-ranked galaxy exhibit values of T1 and T2 lower than unity. According to Mamon (1987), mergers within groups reduce the values of T1 and T2 below 0.7. Finally, we split the samples of CGs into physically dense (Reals) and chance alignments (CAs) following the 3D classification performed by Díaz-Giménez & Mamon (2010) which involves s_4, $s_\perp$ and $s_\parallel$.

The median of these properties and the percentages of Reals CGs are quoted in Table 2. The shifts to compute the 95% confidence interval (CI) for the median are quoted within parentheses, and are given by $1.58 \times IQR/\sqrt{n}$, where n is the number of objects in the sample and IQR is the interquartile range (Krzywinski & Altman 2014).

Using the non-parametric Kolmogorov-Smirnov test, we measured the probability that two samples are drawn from the same distribution. In Table 3, we quote the p-values obtained from the test when comparing pairs of samples. We have highlighted the cells when the probability is lower than a typical critical value of 0.05, which indicates statistical differences for the distributions of a given property between the two samples.

Table 3. P-values of the Kolmogorov-Smirnov two sample test. Each column combines different pairs of CG samples: the first three columns compare the total samples, the following three columns compare the restricted samples, while the last three columns compare the total vs restricted samples in each band. We highlighted in grey the cells with p-values lower than 0.05.

	K - r	K - u	u - r	$\widetilde{\rm K}$ - $\tilde{\rm r}$	$\widetilde{\rm K}$ - $\tilde{\rm u}$	$\tilde{\rm u}$ - $\tilde{\rm r}$	K - $\widetilde{\rm K}$	r - $\tilde{\rm r}$	u - $\tilde{\rm u}$
θ_G	0.16	0.08	0.32	$4{\rm x}10^{-3}$	0.72	0.19	1.00	0.11	1.00
r_p	0.02	0.99	0.13	$7{\rm x}10^{-3}$	0.56	$1{\rm x}10^{-3}$	1.00	1.00	0.51
$R_{\rm vir}$	$1{\rm x}10^{-4}$	0.06	0.19	$3{\rm x}10^{-5}$	0.18	0.05	0.97	1.00	0.66
$\langle d_{ij}\rangle$	0.01	0.42	0.12	$2{\rm x}10^{-3}$	0.47	$4{\rm x}10^{-3}$	0.98	1.00	0.31
$s_\perp$	0.02	0.23	0.87	0.04	0.57	0.14	0.99	1.00	0.29
$s_\parallel$	0.56	$5{\rm x}10^{-4}$	0.02	0.68	$9{\rm x}10^{-3}$	0.26	1.00	1.00	0.79
s_4	0.26	$3{\rm x}10^{-3}$	0.06	0.24	0.10	0.75	1.00	1.00	0.68
σ_v	1.00	0.23	0.24	0.72	0.94	0.66	0.99	1.00	1.00
$H_0\,t_{\rm cr}$	0.19	0.09	0.88	0.41	0.96	0.36	1.00	1.00	0.55
$\mathcal{M}_{\rm vir}$	0.45	0.40	0.27	0.08	0.78	0.70	0.91	1.00	1.00
$K_{\rm bri}$	$1{\rm x}10^{-5}$	0.01	$1{\rm x}10^{-4}$	0.93	0.29	0.26	0.10	$1{\rm x}10^{-7}$	0.03
$r_{\rm bri}$	$1{\rm x}10^{-4}$	0.37	$1{\rm x}10^{-4}$	0.95	0.25	0.37	0.03	$1{\rm x}10^{-8}$	0.06
$u_{\rm bri}$	$8{\rm x}10^{-3}$	$2{\rm x}10^{-3}$	$1{\rm x}10^{-5}$	0.99	0.20	0.60	0.01	$6{\rm x}10^{-8}$	1.00
ΔK_{12}	0.04	$1{\rm x}10^{-3}$	0.18	0.24	0.03	0.71	1.00	0.96	0.96
Δr_{12}	0.08	$1{\rm x}10^{-3}$	0.25	0.35	0.01	0.64	1.00	1.00	1.00
Δu_{12}	0.11	0.03	0.99	0.35	0.01	0.64	1.00	1.00	1.00
μ_K	$4{\rm x}10^{-3}$	0.10	0.20	$7{\rm x}10^{-3}$	0.72	$1{\rm x}10^{-3}$	0.97	1.00	0.19
μ_r	$4{\rm x}10^{-3}$	0.19	0.13	$5{\rm x}10^{-3}$	0.39	$1{\rm x}10^{-3}$	0.94	1.00	0.23
μ_u	0.01	0.50	0.04	0.01	0.26	$1{\rm x}10^{-3}$	0.86	1.00	0.59
L_K	0.73	$8{\rm x}10^{-3}$	0.14	0.87	0.24	0.56	1.00	1.00	0.75
L_r	0.75	0.03	0.17	0.89	0.50	0.51	1.00	1.00	1.00
L_u	1.00	0.79	0.73	0.79	0.99	0.80	1.00	1.00	0.96
$\mathcal{M}_{\rm v}/L_K$	0.29	0.11	0.76	0.10	0.19	0.97	0.99	1.00	0.97
$\mathcal{M}_{\rm v}/L_r$	0.34	0.20	0.91	0.12	0.29	1.00	0.99	1.00	1.00
$\mathcal{M}_{\rm v}/L_u$	0.39	0.73	0.51	0.21	0.48	0.91	0.97	1.00	1.00

Analysing the values of the medians (Table 2) and the comparison between the properties in different photometric bands (Table 3) we found:

- K-CGs have projected sizes (r_p,$R_{\rm vir}$, d_{ij}) statistically smaller than r-CGs.
- K-CGs show smaller 3D interparticle separation (s_4) than the u-CGs.
- u-CGs present the lowest velocity dispersion (although the difference is not significant)
- the magnitude gap in the three bands is larger for the K-CGs than for the u-CGs.
- K-CGs show greater compactness (lower surface brightness) in the three bands than the r-CGs, and similar to the u-CGs (except for μ_u).
- the luminosity in the u-band is similar for CGs identified in any of the three bands. However, the K-band and r-band luminosities of the K-CGs are higher than the luminosities of the u-CGs.
- the brightest galaxies of the u-CGs are brighter than the brightest galaxies of the K- or r-CGs in the three bands.
- The T_1 and T_2 computed in the K- and r- band show very low values for the K-CGs and r-CGs samples which means very different first and second-ranked galaxies in luminosity, indicating clear signals of mergers within groups. Even though the u-CGs show T_1 and T_2 below the unity, their values are close to 0.7.
- the K-CG sample comprises more Real CGs than the observed in the other photometric bands. The lowest value for the percentage of Real CGs is obtained in the u-CG sample.

Díaz-Giménez et al. (2012) and Hernández-Fernández & Mendes de Oliveira (2015) compared CGs identified in different bands and with different algorithms. Regarding the projected sizes, both studies agreed that groups identified in the R- (Hickson et al. 1992; Allam & Tucker 2000) or r- band (McConnachie et al. 2009) where smaller in projection than groups identified in the K-band (Díaz-Giménez et al. 2012), and Hernández-Fernández & Mendes

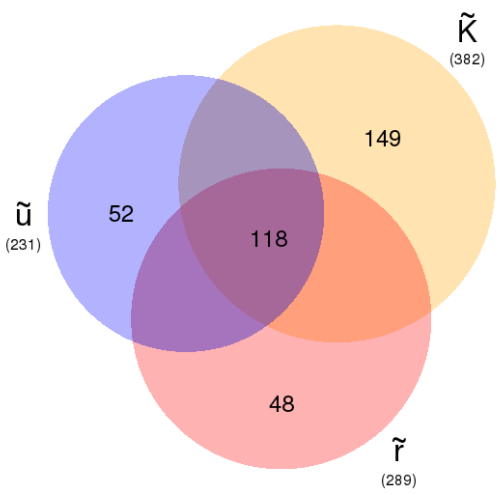

Figure 2. Schematic Venn diagrams that shows the different overlapping regions that are obtained when comparing the group identified on each photometric band. The number of groups in the total restricted samples are quoted in parentheses. The number of groups identified only in a given band and those that are common in the three bands are also quoted inside the coloured circles.

de Oliveira also stated that their UV-CGs are the smallest. In this work we found a different result: K-CGs and u-CGs are smaller than r-CGs. This controversial result might be expected since the difference in the algorithms used to identify the observational samples that have been compared introduce the differences in sizes reported in the literature. Using friends-of-friends algorithms, or Hickson-like criteria based on the projected sizes, and also including/excluding the CG-in-CG options introduces a bias in the projected sizes of the resulting groups. In this work, we avoided this issue by using the same algorithm in the three photometric bands, therefore the results reported here are only due to intrinsic differences between bands. Also, Díaz-Giménez et al. (2012) and Hernández-Fernández & Mendes de Oliveira (2015) found that the crossing times of groups identified in the B and UV bands are larger than K-CGs which in turn are larger than R- or r-CGs. Here, we do not find significant differences between the crossing times of groups identified in the three bands. Moreover, Díaz-Giménez et al. (2012) found that the mean projected interparticle separation between galaxies in R-CGs is smaller than in K-CGs, which are smaller than B-CGs. However, Hernández-Fernández & Mendes de Oliveira (2015) found that the smallest interparticle separation was in the UV-CGs, with the r-CGs presenting the largest separations. In this work we found the r-CGs with the largest interparticle separation in agreement with Hernández-Fernández & Mendes de Oliveira (2015). Finally, Díaz-Giménez et al. (2012) found that the only sample showing T1 and T2 values below unity was the one identified in the K-band. On the contrary, in this work using the same algorithm in the three bands, we do find that all the values are below unity, being higher in the u-band and very similar in the K- and r-bands.

2.4 Restricted samples

One may wonder whether the differences we found in the previous section could be biased due to the fact that each sample has been selected with different criteria depending on the band ($\mu_{\rm lim}$ and $m_{\rm bri_{lim}}$). Therefore, in this section we normalised the criteria to avoid any dependence on the selection function.

We defined the "restricted" samples ($\widetilde{\rm K}$-, r̃- and ũ-CGs) by selecting CGs in each catalogue that also satisfy the compactness and flux criteria in the other two bands. For instance, the $\widetilde{\rm K}$-CGs are a subsample of the K-CGs that also satisfy that $\mu_{\rm r} < 26.33$, and $\mu_{\rm u} < 28.65$, and $r_{\rm brightest} < 13.54$, and $u_{\rm brightest} < 15.73$. We selected the r̃- and ũ-CGs in a similar way.

We found that 85.5% of the K-CGs survive the triple restriction, while 71.2% of the r-CGs and 83.7% of the u-CGs conform their restricted samples. In Table 2 we quoted the medians of the properties of these restricted samples and the quantities to compute their 95% confidence interval, while in Table 3 we quoted the p-values obtained from the KS-test used for the comparison between samples.

In general, the restricted samples only differ from the original samples in those properties that are explicitly dependent on the limit adopted on the magnitudes (see the last three columns of Table 3). As a consequence, the differences we found between the original samples in the magnitude of the brightest galaxies and total luminosities of the groups are not longer present once we imposed the same limits for the three catalogues.

However, the differences in sizes, magnitude gaps and surface brightness remain in the restricted samples: ũ-CGs are smallest in projection, the K-CGs have the largest magnitude gap (although non-significant compared to r̃-CGs), while the r̃-CGs have the largest surface brightness -lower compactness- and this result is more significant now using the restricted samples.

As a by product, having restricted the samples in the three bands at the same time has slightly increased the probability of selecting physically dense groups (Reals) in the K and u bands, which is something desirable in an observational sample where we cannot easily distinguish between chance alignments and physically dense groups.

3 CROSS-IDENTIFIED COMPACT GROUPS: PURE AND COMMON IDENTIFICATIONS

Although the CGs belonging to the restricted samples accomplish the compactness and flux criteria in the three bands at the same time, those groups are not the same. In Fig. 2 we show the Venn diagram of the three sets of restricted groups. In this section we are interested in analysing the CGs that can be identified in the three bands at the same time and those CGs that can be identified only in one particular band.

To select CGs that were identified in the three bands, we first looked for CGs that were identified in two bands at the same time, and then we cross-checked if those groups were also in the third band. When comparing CGs in two bands, there could be CGs that belonging to both catalogues are not necessarily exactly the same: there could be a slightly different number of members in the two bands by including/excluding a galaxy in one or the other band. Therefore, instead of making a member-to-member comparison, we adopted a simpler criterion to determine whether a CG that belongs to two different catalogues is the same: if the angular distance between the centres of the minimum circles is less than twice the

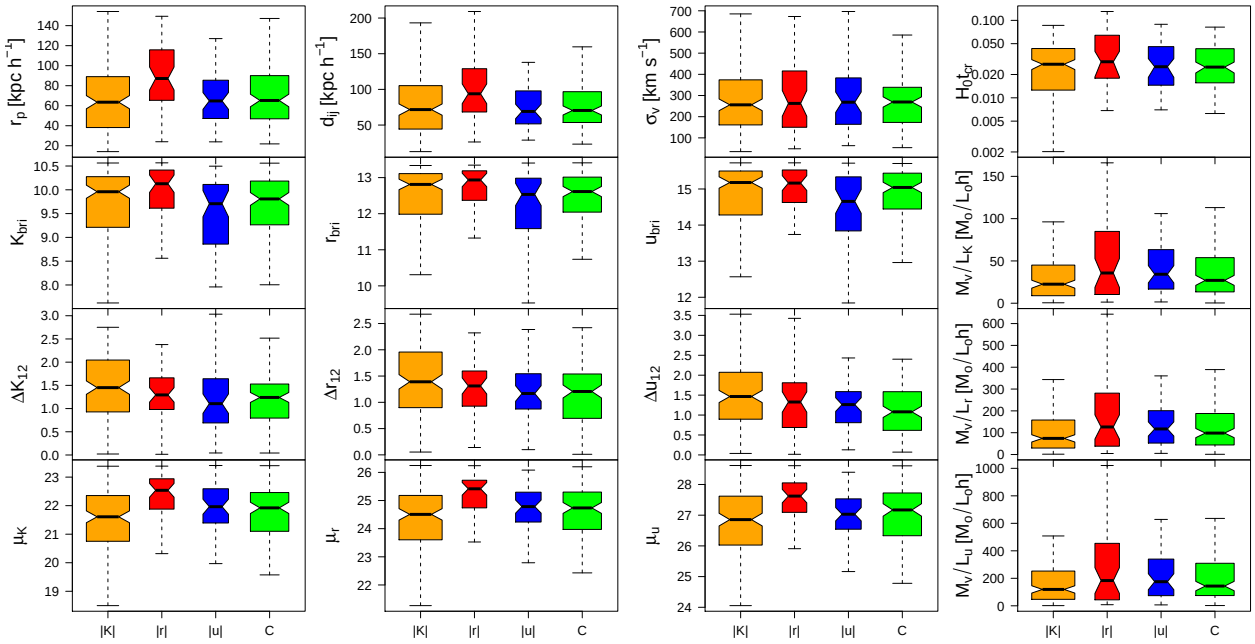

Figure 3. Boxplot diagrams of some of the properties for the pure and common CGs. The notches indicates the approximate 95% confidence interval for the medians, while the widths are proportional to the square roots of the number of CGs in each sample. The complete list of values for the medians and their corresponding 95% confidence intervals for all the properties studied in this work are quoted in Table A1.

angular radius of the CG and the difference in radial velocity of the centres is less than $1000\,\mathrm{km\,s^{-1}}$. Using this criterion we found 118 CGs in common in the three bands (C-CGs). They represent 31% of the $\widetilde{\mathrm{K}}$-CGs, 41% of the $\tilde{\mathrm{r}}$-CGs and 51% of the $\tilde{\mathrm{u}}$-CGs.

On the other hand, CGs in each band that have not a counterpart in any of the other two catalogues conform the sample of "pure" CGs ($|K|$-,$|r|$-,$|u|$-CGs). We found that $\sim$ 39% of the $\widetilde{\mathrm{K}}$-CGs can only be identified when analysing a sample of galaxies selected in the K-band, $\sim$ 17% of the $\tilde{\mathrm{r}}$-CGs exist only in the r-band, while $\sim$ 23% of the $\tilde{\mathrm{u}}$-CGs exist only in the u-band.

We show a comparison of some of the properties of CGs belonging to each of these subsamples using boxplot diagrams in Fig. 3. In these diagrams, the notches correspond to the approximated 95% confidence intervals. In general, when notches do not overlap, the medians can be judged to differ significantly (Krzywinski & Altman 2014), but overlap does not rule out a significant difference. In appendix A, we show the values of the medians and their confidence intervals for all the properties used in this work for groups in each of these samples, as well as the p-values of the KS-tests between pairs of samples (Tables A1 and A2, respectively).

From the analysis of the properties (see Fig. 3 and Tables A1) for the different CG samples in different photometric bands we can mention the following highlights:

- $|K|$-CGs present the smallest projected virial radius, virial masses, surface brightness (highest compactness), mass-to-light ratios and the largest magnitude gaps, even larger than all the samples previously analysed. They also produce the lowest values of T1 and T2.
- $|r|$-CGs present the largest projected sizes, virial masses, surface brightness (lowest compactness), and mass-to-light ratios.
- $|u|$-CGs present the brightest first ranked galaxy, and the largest 3D and line-of-sight interparticle separations (which makes the $|u|$ sample to present the lowest percentage of physically dense groups - according to our criterion based on the 3D comoving separations). On average, these groups show one of the largest values of T1 and T2.
- C-CGs present the smallest 3D, line-of-sight and projected comoving sizes of the four closest neighbours (which implies having the largest fraction of Real CGs).

By comparing Table A2 and Table 3, we can analyse the effect of including/excluding groups that exist in one or other band. In general, the differences found between restricted CGs remain, but also a few other differences arise when comparing pure vs pure samples that were not present in the restricted samples. We found that $|K|$ virial masses are significantly lower than $|r|$ virial masses, and this is also observed when analysing the mass-to-light ratios. In addition, the 3D comoving interparticle separations of $|u|$-CGs are statistically larger than for the $|K|$-CGs. Also, the brightest galaxies (in any band) of the $|r|$-CGs are typically brighter than the brightest galaxies in $|u|$-CGs.

Finally, when comparing the pure CGs with the common CGs we found a couple of differences with one or other sample. The projected sizes of C-CGs are quite similar to the $|u|$, however, the 3D interparticle separations of the C-CGs are significantly smaller than the $|u|$. The magnitude gaps in the three bands of the $|K|$ sample are typically larger than the gaps for the common groups, meaning the common CGs are conformed by more similar neighbour galaxies than the pure K. The $|r|$-CGs are statistically less "compact" (fainter μ) than the common CGs. Also, the brightest galaxies in C-CGs are brighter than their counterpart in $|r|$-CGs. Interestingly, the common CGs present the largest percentage of Real CGs. This is a novel result that may help selecting observational samples with the lowest percentage of chance alignments, although it is necessary to have data in multiple photometric bands. Some of the differences that we found between the samples of "pure" CGs are not observed in the restricted samples given the existence of the com-

mon CGs that either in some cases represent a high percentage of the restricted samples or that they properties are placed in between the values of the extreme pure samples, blurring the differences in the restricted sample.

4 SUMMARY

In this work we aimed to analyse whether the differences reported in the literature between compact groups identified in different bands are still present when a single finding algorithm is applied on samples of galaxies selected in different photometric bands. Therefore, we worked with the synthetic galaxies from the galaxy lightcone built by Henriques et al. (2012), which combines the galaxies from the semi-analytic model of galaxy formation of Guo et al. (2011) and the dark-matter particles of the Millennium Run Simulation (Springel et al. 2005). We note that adopting any specific semi-analytic model could introduce a dependence of the results on the particular set of parameters and physical processes that were used in the model construction. Nevertheless, this lightcone is one of the very few freely available mock catalogues that provides apparent magnitudes in nine photometric bands obtained for galaxies extracted from a high resolution N-body simulation, which makes this sample ideal for performing comparative studies between properties of compact groups in different bands. Moreover, this particular semi-analytic model has proven to be quite efficient at reproducing the observed abundance of low redshift galaxies over a wide range of stellar masses and luminosities, and also the large-scale clustering as a function of stellar masses and galaxy colours (Guo et al. 2011). Differences with observations have been indeed reported for the population of galaxies at $z \geqslant 1$, which is far outside the redshift range of interest in this work. Analysing the differences in mock compact groups caused by using different semi-analytic models is beyond the scope of this work, and it has been previously assessed by Díaz-Giménez & Mamon (2010).

From the original lightcone, we built three mock catalogues in different photometric bands (K, r and u) by selecting galaxies brighter than an given apparent magnitude limit. We adopted the K-band apparent magnitude limit to mimic the observational sample of galaxies of the 2MASS ($K_{\rm lim} = 13.57$). By analysing the magnitude-magnitude distribution of galaxies in the lightcone, we determined the limits in the other two bands to be equivalent to the limit in the K-band ($r_{\rm lim} = 16.4$ and $u_{\rm lim} = 18.73$).

We identified compact groups in each of the three mock catalogues by applying an automatic Hickson-like algorithm. At first, this algorithm identifies compact groups in projection. The criteria include membership, compactness, isolation and flux limit. The limiting values for each of these criteria have to be changed according to the photometric band in order to obtain similar results. Once the compact groups have been selected in projection, the algorithm performs a velocity filtering to avoid many interlopers. We found 447 K-CGs, 406 r-CGs and 276 u-CGs.

The comparison of properties of CGs identified in the three bands revealed that K-CGs and u-CGs present smaller projected radii than r-CGs, however, analysing the 3D comoving interparticle separations between the four closest members, the u-CGs have the longest separations while the K-CGs have the shortest. We do not find differences in crossing times between the three samples of CGs. Most of these results are in conflict with previous comparisons reported in the literature (Díaz-Giménez et al. 2012; Hernández-Fernández & Mendes de Oliveira 2015). The main reason for these discrepancies is due to the difficult task of comparing groups samples identified with different algorithms (Hickson-visual inspection or FoF like) that could bias the resulting group properties, particularly the sizes which are part of the finding criteria.

We also found that the brightest galaxy in u-CGs tends to be brighter than the brightest galaxies in r- or K-CGs. The magnitude gap between the two brightest galaxies in a group is larger for K-CGs than for u-CGs. The r-CGs present the highest values of surface brightness in any of the three bands, which means a lowest "compactness".

We have checked if these results were dependent on the different choices of the band-dependent limiting values in the identification criteria. Therefore, we defined "restricted" samples of CGs in the three bands by restricting the samples using also the limiting values of the other two bands (e.g., the restricted r-CGs accomplish the μ_r and $r_{\rm bri}$ criteria, and also the μ_K, μ_u, $K_{\rm bri}$ and $u_{\rm bri}$ criteria). We confirmed that u-CGs are the smallest in projection, the K-CGs have the largest magnitude gaps and the smallest 3D interparticle separations, while the r-CGs have the highest surface brightness and the largest projected sizes. Several of these results have been enhanced in the restricted sample in comparison with the results obtained for the total samples.

Although we intended to normalise the criteria, the samples of CGs are still different. Not all the CGs identified in one band are also present in the other bands. In order to disentangle more specifically which differences are intrinsically due to the photometric band in which the galaxies were observed, from the samples of restricted CGs we selected those groups that are common in the three identification and those that only exist in one of the mock catalogues (pure CGs). The common CGs are half of the restricted u-CGs (51%), while they represent only 1/3 of the K-CGs, and we found a percentage in between for the r-CGs (41%). Groups that are only identified in the K-band represent 39% of the restricted K-CGs, while the percentage of "pure-r" CGs represent 17% of the restricted r-CGs, and 23% of the restricted u-CGs are identifiable only in the u-band.

The comparison between these samples indicates that pure-r CGs are the largest in projection, and they also have the highest surface brightness (less compact). The pure-u CGs have the brightest first ranked galaxies, and the smallest differences between the first and the second ranked galaxies. The pure-K CGs have the highest compactness and the smallest virial masses, and mass-to-light ratios. More noticeable, this sample presents the largest magnitude gaps between the two brightest group members when compared with all the sample of CGs used in this work. This result is a clear indication that this characteristic is inherent of groups only identified in this particular photometric band. This result is also related with the very low values obtained for the Tremaine-Richstone statistics, T1 and T2, which are commonly thought as indication of galaxy mergers. Finally, the CGs that are in common in the three bands present the smallest 3D comoving galaxy separations between the four closest galaxies, which makes them very compact physical entities in 3D space, therefore, this sample shows the largest percentage of Real CGs (using Díaz-Giménez & Mamon 2010 definition of Reals).

Our results indicate that the comparison of compact groups from different sources has to be done carefully to avoid introducing biases related to the different selection functions, but we also demonstrated that there are indeed intrinsic features that differ from band to band. Some of those differences can be blurred in the bulk of data given the existence of compact groups common to all the photometric bands. Despite these results were obtained from one

single semi-analytic model of galaxy formation, this model reproduces very well the observable local luminosity function in the K, r and u photometric bands, and also the clustering of galaxies as a function of stellar masses and colours (Guo et al. 2011; Henriques et al. 2012). Therefore, we are quite confident that the differences we found between the mock CGs in different bands might also mimic the differences between observational CGs. However, the predictions presented in this work need to be confirmed from unbiased studies performed on multi-band observational catalogues, and/or when different models of galaxy formation with information in multiple photometric bands are released.

ACKNOWLEDGEMENTS

The Millennium Simulation databases used in this paper and the web application providing online access to them were constructed as part of the activities of the German Astrophysical Virtual Observatory (GAVO). We thank Bruno Henriques for allowing public access for the outputs of his all-sky mock catalogue and kindly answering questions about the sample. This work has been partially supported by Consejo Nacional de Investigaciones Científicas y Técnicas de la República Argentina (CONICET), PIP: 11220130100365, and the Secretaría de Ciencia y Tecnología de la Universidad de Córdoba (SeCyT), 203/14.

REFERENCES

Allam S. S., Tucker D. L., 2000, Astronomische Nachrichten, 321, 101
Bertone S., Lucia G. D., Thomas P. A., 2007, Monthly Notices of the Royal Astronomical Society, 379, 1143
Bianchi L., 2014, Ap&SS, 354, 103
Cohen M., Wheaton W. A., Megeath S. T., 2003, AJ, 126, 1090
Cousins A. W. J., 1976, MmRAS, 81, 25
Díaz-Giménez E., Mamon G. A., 2010, Monthly Notices of the Royal Astronomical Society, 409, 1227
Díaz-Giménez E., Mamon G. A., Pacheco M., de Oliveira C. M., Alonso M. V., 2012, Monthly Notices of the Royal Astronomical Society, 426, 296
Focardi P., Kelm B., 2002, Astronomy and Astrophysics, 391, 35
Guo Q., White S., Boylan-Kolchin M., Lucia G. D., Kauffmann G., Lemson G., Li C., Springel V., Weinmann S., 2011, Monthly Notices of the Royal Astronomical Society, 413, 101
Henriques B. M. B., White S. D. M., Lemson G., Thomas P. A., Guo Q., Marleau G.-D., Overzier R. A., 2012, Monthly Notices of the Royal Astronomical Society, 421, 2904
Hernández-Fernández J. D., Mendes de Oliveira C., 2015, MNRAS, 453, 1965
Hickson P., 1982, ApJ, 255, 382
Hickson P., Mendes de Oliveira C., Huchra J. P., Palumbo G. G., 1992, ApJ, 399, 353
Johnson H. L., Morgan W. W., 1953, ApJ, 117, 313
Krzywinski M., Altman N., 2014, Nature Methods, 11, 119
Lange R., Driver S. P., Robotham A. S. G., Kelvin L. S., Graham A. W., Alpaslan M., Andrews S. K., Baldry I. K., Bamford S., Bland-Hawthorn J., Brough S., Cluver M. E., Conselice C. J., Davies L. J. M., Haeussler B., Konstantopoulos I. S., Loveday J., Moffett A. J., Norberg P., Phillipps S., Taylor E. N., Lopez-Sanchez A. R., Wilkins S. M., 2015, Monthly Notices of the Royal Astronomical Society, 447, 2603
Mamon G. A., 1987, ApJ, 321, 622
McConnachie A. W., Patton D. R., Ellison S. L., Simard L., 2009, Monthly Notices of the Royal Astronomical Society, 395, 255
Prandoni I., Iovino A., MacGillivray H. T., 1994, AJ, 107, 1235
Rose J. A., 1977, ApJ, 211, 311
Skrutskie M. F., Cutri R. M., Stiening R., Weinberg M. D., Schneider S., Carpenter J. M., Beichman C., Capps R., Chester T., Elias J., Huchra J., Liebert J., Lonsdale C., Monet D. G., Price S., Seitzer P., Jarrett T., Kirkpatrick J. D., Gizis J. E., Howard E., Evans T., Fowler J., Fullmer L., Hurt R., Light R., Kopan E. L., Marsh K. A., McCallon H. L., Tam R., Van Dyk S., Wheelock S., 2006, AJ, 131, 1163
Springel V., White S. D. M., Jenkins A., Frenk C. S., Yoshida N., Gao L., Navarro J., Thacker R., Croton D., Helly J., Peacock J. A., Cole S., Thomas P., Couchman H., Evrard A., Colberg J., Pearce F., 2005, Nature, 435, 629
Targett T. A., Dunlop J. S., McLure R. J., 2012, MNRAS, 420, 3621
Tremaine S. D., Richstone D. O., 1977, ApJ, 212, 311
Yentis D. J., Cruddace R. G., Gursky H., Stuart B. V., Wallin J. F., MacGillivray H. T., Collins C. A., 1992, in Astrophysics and Space Science Library, Vol. 174, Digitised Optical Sky Surveys, MacGillivray H. T., Thomson E. B., eds., p. 67
York D. G., SDSS Collaboration, 2000, AJ, 120, 1579

APPENDIX A: TABLES FOR PURE AND COMMON CGS

In this section we quote tables including the medians and 95% confidence intervals for all the properties under study and the p-values obtained from the comparison among different photometric bands for the samples of pure and common CGs defined in Sect. 3.

Table A1. Group properties for the samples of pure and common CGs

Sample	$\|K\|$	$\|r\|$	$\|u\|$	C
# of CGs	149	48	52	118
θ_G	2.7 (0.3)	4.0 (0.5)	4.0 (0.7)	3.5 (0.3)
r_p	63 (6)	87 (11)	64 (8)	65 (6)
$R_{\rm vir}$	71 (8)	115 (19)	90 (17)	95 (8)
$\langle d_{ij} \rangle$	71 (7)	93 (13)	69 (10)	70 (6)
$s_\perp$	105 (10)	125 (19)	103 (14)	93 (10)
$s_\parallel$	123 (23)	128 (59)	220 (139)	108 (26)
s_4	173 (24)	214 (53)	229 (133)	153 (26)
σ_v	255 (27)	262 (60)	268 (47)	269 (24)
$H_0\, t_{\rm cr}$	2.7 (0.4)	2.9 (1.1)	2.5 (0.7)	2.5 (0.4)
$\mathcal{M}_{\rm vir}$	5.0 (1.1)	8.7 (5.8)	7.6 (2.4)	6.1 (1.7)
$K_{\rm bri}$	10.0 (0.1)	10.1 (0.2)	9.7 (0.3)	9.8 (0.1)
$r_{\rm bri}$	12.8 (0.1)	12.9 (0.2)	12.5 (0.3)	12.6 (0.1)
$u_{\rm bri}$	15.2 (0.2)	15.2 (0.2)	14.7 (0.3)	15.0 (0.1)
ΔK_{12}	1.5 (0.1)	1.3 (0.2)	1.1 (0.2)	1.2 (0.1)
Δr_{12}	1.4 (0.1)	1.3 (0.2)	1.2 (0.1)	1.2 (0.1)
Δu_{12}	1.5 (0.2)	1.3 (0.3)	1.3 (0.2)	1.1 (0.1)
μ_K	21.6 (0.2)	22.5 (0.2)	22.0 (0.3)	21.9 (0.2)
μ_r	24.5 (0.2)	25.4 (0.2)	24.8 (0.2)	24.7 (0.2)
μ_u	26.9 (0.2)	27.6 (0.2)	27.0 (0.2)	27.2 (0.2)
L_K	231 (23)	197 (68)	196 (32)	224 (24)
L_r	66 (6)	63 (18)	58 (9)	64 (7)
L_u	41 (5)	40 (15)	41 (7)	41 (4)
$\mathcal{M}_{\rm v}/L_K$	22 (4)	35 (17)	34 (10)	27 (5)
$\mathcal{M}_{\rm v}/L_r$	73 (16)	126 (55)	117 (32)	98 (20)
$\mathcal{M}_{\rm v}/L_u$	119 (26)	183 (93)	175 (58)	143 (34)
$T1_K$	0.53 (0.04)	0.53 (0.07)	0.67 (0.09)	0.55 (0.04)
$T2_K$	0.60 (0.04)	0.60 (0.07)	0.72 (0.08)	0.58 (0.04)
$T1_r$	0.50 (0.03)	0.56 (0.07)	0.62 (0.07)	0.57 (0.05)
$T2_r$	0.55 (0.03)	0.60 (0.06)	0.61 (0.07)	0.62 (0.05)
$T1_u$	0.56 (0.04)	0.71 (0.06)	0.72 (0.08)	0.58 (0.05)
$T2_u$	0.62 (0.04)	0.73 (0.08)	0.59 (0.07)	0.66 (0.05)
% Reals	53.7	45.8	40.4	59.3

Notes: In each cell, the format xx (ss) contains the median (xx) and the shift (ss) to construct an approximated 95% confidence interval, $CI = xx \pm ss$ (see text for details), except for the T_1 and T_2 values where the quantity in parentheses are the error bars computed using the bootstrap resampling technique. Units: θ_G = $arcmin$; r_p, $R_{\rm vir}$, $< d_{ij} >$, $s_\perp$, $s_\parallel$ and s_4 = $kpc\ h^{-1}$; σ_v = $km\ s^{-1}$; $H_0\, t_{\rm cr}$ = 10^{-2} ; $\mathcal{M}_{\rm vir}$ = $10^{12}\ M_\odot\ h^{-1}$;magnitude gaps are calculated in absolute magnitudes for each photometric band; μ = $mag/arcsec^2$; L = $10^9\ L_\odot\ h^{-2}$; $\mathcal{M}_{\rm vir}/L$ = $M_\odot/L_\odot\ h$.

Table A2. P-values of the Kolmogorov-Smirnov two sample test. Each column combines different pairs of pure and common CG samples. Grey shaded cells are included to highlight p-values lower than 0.05.

	$\|K\|$ - $\|r\|$	$\|K\|$ - $\|u\|$	$\|u\|$ - $\|r\|$	$\|K\|$ - C	$\|r\|$ - C	$\|u\|$ - C
θ_G	$2\text{x}10^{-4}$	0.02	0.43	$3\text{x}10^{-3}$	0.23	0.21
r_p	$2\text{x}10^{-3}$	0.58	0.01	0.10	$7\text{x}10^{-3}$	0.95
$R_{\rm vir}$	$2\text{x}10^{-4}$	0.12	0.09	$3\text{x}10^{-5}$	0.20	0.14
$\langle d_{ij} \rangle$	$1\text{x}10^{-3}$	0.35	$4\text{x}10^{-3}$	0.17	$7\text{x}10^{-4}$	1.00
$s_\perp$	0.04	0.62	0.20	0.60	$4\text{x}10^{-3}$	0.36
$s_\parallel$	0.82	$4\text{x}10^{-3}$	0.13	0.88	0.44	$5\text{x}10^{-3}$
s_4	0.28	0.02	0.13	0.66	0.16	0.01
σ_v	0.77	0.73	0.93	0.38	0.28	0.30
$H_0\, t_{\rm cr}$	0.09	0.83	0.35	0.15	0.34	0.97
$\mathcal{M}_{\rm vir}$	0.02	0.27	0.26	0.20	0.12	0.84
$K_{\rm bri}$	0.15	0.13	0.02	0.20	0.03	0.39
$r_{\rm bri}$	0.22	0.08	0.03	0.06	0.04	0.39
$u_{\rm bri}$	0.84	0.03	0.04	0.28	0.59	0.08
ΔK_{12}	0.12	0.07	0.20	$3\text{x}10^{-3}$	0.49	0.97
Δr_{12}	0.18	0.01	0.66	$1\text{x}10^{-4}$	0.22	0.42
Δu_{12}	0.18	0.01	0.66	$1\text{x}10^{-4}$	0.22	0.42
μ_K	$2\text{x}10^{-5}$	0.03	$7\text{x}10^{-3}$	0.07	$2\text{x}10^{-4}$	0.34
μ_r	$6\text{x}10^{-5}$	0.06	0.01	0.15	$2\text{x}10^{-4}$	0.34
μ_u	$5\text{x}10^{-4}$	0.22	$9\text{x}10^{-3}$	0.10	$2\text{x}10^{-3}$	0.79
L_K	0.39	0.39	0.83	0.69	0.11	0.42
L_r	0.53	0.56	0.68	0.73	0.26	0.31
L_u	0.30	0.80	0.46	0.66	0.08	0.60
$\mathcal{M}_{\rm v}/L_K$	0.03	0.07	0.67	0.29	0.06	0.44
$\mathcal{M}_{\rm v}/L_r$	0.04	0.11	0.67	0.29	0.21	0.59
$\mathcal{M}_{\rm v}/L_u$	0.06	0.20	0.64	0.20	0.26	0.96